

Full length article

Triple drugs co-delivered by a small gemcitabine-based carrier for pancreatic cancer immunochemotherapy[☆]

Jingjing Sun^{a,b,*}, Zhuoya Wan^{a,b}, Yichao Chen^{a,b}, Jieni Xu^{a,b}, Zhangyi Luo^{a,b},
Robert A. Parise^{c,d}, Dingwei Diao^{a,b}, Pengfei Ren^{a,b}, Jan H. Beumer^{c,d}, Binfeng Lu^e,
Song Li^{a,b,**}

^a Center for Pharmacogenetics, School of Pharmacy, University of Pittsburgh, Pittsburgh, PA, USA

^b Department of Pharmaceutical Sciences, School of Pharmacy, University of Pittsburgh, Pittsburgh, PA, USA

^c Cancer Therapeutics Program, UPMC Hillman Cancer Center, Pittsburgh, PA, USA

^d Division of Hematology-Oncology, Department of Medicine, University of Pittsburgh School of Medicine, Pittsburgh, PA, USA

^e Department of Immunology, University of Pittsburgh School of Medicine, Pittsburgh, PA, USA

ARTICLE INFO

Article history:

Received 20 November 2019

Revised 23 January 2020

Accepted 23 January 2020

Available online 28 January 2020

Keywords:

PDA

Immunotherapy

Indoleamine 2

3-dioxygenase-1

Penetration

Drug delivery

ABSTRACT

Poor tumor penetration and highly immunosuppressive tumor microenvironment are two major factors that limit the therapeutic efficacy for the treatment of pancreatic ductal adenocarcinoma (PDA). In this work, a redox-responsive gemcitabine (GEM)-conjugated polymer, PGEM, was employed as a tumor penetrating nanocarrier to co-load an immunomodulating agent (NLG919, an inhibitor of indoleamine 2,3-dioxygenase 1 (IDO1) and a chemotherapeutic drug (paclitaxel (PTX)) for immunochemo combination therapy. The NLG919/PTX co-loaded micelles showed very small size of ~15 nm. *In vivo* tumor imaging study indicated that PGEM was much more effective than the relatively large-sized PEG-co-PVD nanoparticles (~160 nm) in deep tumor penetration and could reach the core of the pancreatic tumor. PTX formulated in the PGEM carrier showed improved tumor inhibition effect compared with PGEM alone. Incorporation of NLG919 in the formulation led to a more immunoactive tumor microenvironment with significantly decreased percentage of Treg cells, and increased percentages of CD4⁺ IFN γ ⁺ T and CD8⁺ IFN γ ⁺ T cells. PGEM micelles co-loaded with PTX and NLG919 showed the best anti-tumor activity in pancreatic (PANC02) as well as two other tumor models compared to PGEM micelles loaded with PTX or NLG919 alone, suggesting that codelivery of NLG919 and PTX via PGEM may represent an effective strategy for immunochemotherapy of PDA as well as other types of cancers.

Statement of Significance

In order to effectively accumulate and penetrate the PDA that is poorly vascularized and enriched with dense fibrotic stroma, the size of nanomedicine has to be well controlled. Here, we reported an immunochemotherapy regimen based on co-delivery of GEM, PTX and IDO1 inhibitor NLG919 through an ultra-small sized GEM-based nanocarrier (PGEM). We demonstrated that the PGEM carrier was effective in accumulating and penetrating into PDA tumors. Besides, PGEM co-loaded with PTX and NLG919 induced an improved anti-tumor immune response and was highly efficacious in inhibiting tumor growth as well as in prolonging the survival rate in PANC02 xenograft model. Our work represents a potential strategy for enhancing PDA tumor penetration and immunochemotherapy.

© 2020 Acta Materialia Inc. Published by Elsevier Ltd. All rights reserved.

1. Introduction

As one of the most difficult-to-treat cancers, pancreatic ductal adenocarcinoma (PDA) is projected to become the second leading cause of cancer-related deaths by 2030 [1]. The standard chemotherapeutic drug for the first-line treatment of PDA is gemcitabine (GEM), which is a cytidine analogue that inhibits DNA

[☆] Author information: All authors have given approval to the final version of the manuscript.

* Corresponding author at: Center for Pharmacogenetics, Department of Pharmaceutical Sciences, School of Pharmacy, University of Pittsburgh, Pittsburgh, PA, 15261, USA.

** Corresponding author at: Center for Pharmacogenetics, Department of Pharmaceutical Sciences, School of Pharmacy, University of Pittsburgh, Pittsburgh, PA, 15261, USA.

E-mail addresses: jis84@pitt.edu (J. Sun), sol4@pitt.edu (S. Li).

<https://doi.org/10.1016/j.actbio.2020.01.039>

1742-7061/© 2020 Acta Materialia Inc. Published by Elsevier Ltd. All rights reserved.

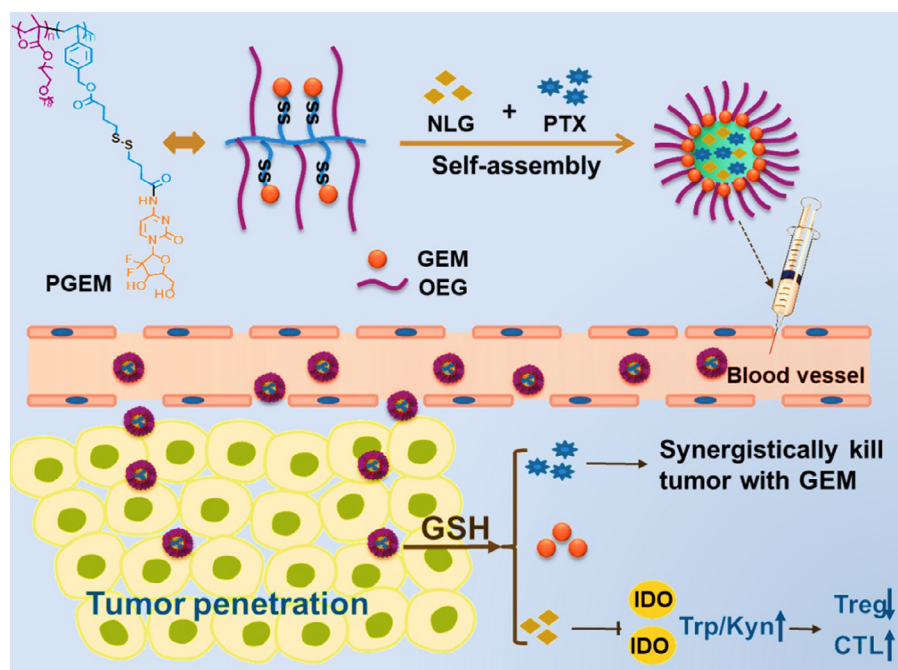


Fig. 1. Schematic illustration of multi-functional PGEM NPs for co-delivery and intracellular GSH-responsive release of PTX, GEM and NLG919. PTX shows synergistic tumor killing effect with GEM. NLG919 would inhibit IDO1 expression and reactivate the immune system. (The NLG919 was shortened to NLG in the following figures).

replication [2]. However, its therapeutic effectiveness is hindered by its rapid metabolism through cytidine deaminase (CDA) [3]. Thus, in clinical practice, GEM is often combined with other therapeutics (such as nab-paclitaxel) to improve the therapeutic effect. Paclitaxel (PTX), in addition to its direct cytotoxic effect on tumor cells, reduces CDA expression and increases GEM accumulation in tumors, leading to a synergistic tumor killing effect with GEM [4,5]. In addition, treatment with PTX and/or GEM can stimulate an antitumor immune response through presentation of antigens released from dying tumor cells or directly killing immunosuppressive cells, which also contributes to the overall antitumor activity [6–8].

Despite these advances, the overall success of PDA treatments remains unsatisfactory, in part due to the persistent highly immunosuppressive pancreatic tumor microenvironment (TME), which assists tumors in evading normal immune surveillance, for instance through upregulation of immune checkpoint molecules, cytotoxic T-lymphocyte-associated antigen 4 (CTLA4) and programmed cell death protein 1 (PD1) [9,10]. Indoleamine 2, 3-dioxygenase (IDO) is another well-characterized immunosuppressive molecule that is overexpressed in pancreatic cancer [11–13]. High expression of IDO1 is correlated with a worse prognosis in pancreatic cancer patients [14,15]. IDO1 works through the degradation of tryptophan into kynurenine, which is toxic to effector T cells and induces recruitment of T regulatory cells (Treg), resulting in the suppression of anti-tumor immune responses [16,17]. Thus, inhibition of IDO1 combined with standard chemotherapy (GEM/PTX) is an attractive strategy for the treatment of PDA.

NLG919 is a potent and specific IDO1 inhibitor with a low EC_{50} [18]. Due to its poor solubility and distinct physical properties from other chemotherapeutic agents, it is difficult to co-deliver NLG919 and other chemotherapeutic agents to tumors. Our group previously developed a NLG919 prodrug (PEG2K-Fmoc-NLG919) as a dual-functional carrier to encapsulate PTX for combination treatment of breast cancer [19]. However, the system is only suitable for codelivery of water-insoluble drugs, and co-delivery of PTX with water-soluble drug like GEM cannot be achieved. Moreover, PEG2K-Fmoc-NLG919-micelles have a relatively large hydrodynamic

size of around 100 nm, which is not suitable for penetrating into the poorly vascularized and stroma-rich PDA tumors.

Vessels in tumors are generally leaky compared with normal vessels, which allow particles of 4–200 nm to selectively accumulate in tumors [20–22]. However, the cutoff pore size varies significantly with the tumor type, and PDA is known to be poorly vascularized with much smaller pore sizes (~50–60 nm) compared to other cancer types [23]. In addition, PDA has dense stroma that further limits the penetration of large nanoparticles (NPs). As a result, small particles with size lower than 50 nm are more suitable for penetrating pancreatic tumors [24]. However, small-sized NPs often showed lower drug loading capacity and efficiency compared to larger NPs [25–28]. It remains a challenge to develop a small-sized nanocarrier that is capable of deep tumor penetration yet highly effective in codelivery of different drugs (such as GEM/PTX and NLG919) for PDA immunochemotherapy.

We recently found that conjugation of GEM to PEOG-co-PVD polymer could significantly reduce the size of resultant polymeric micelles and improve the drug loading capacity due to the hydrogen bonding effect [29]. In this work, we evaluated the efficiency of the GEM-based prodrug carrier (PGEM) in co-delivering IDO inhibitor NLG919 and chemotherapeutic drugs PTX/GEM into pancreatic tumor for immunochemotherapy (Fig. 1). It is hypothesized that due to the ultra-small size effect, the PGEM micelles co-loaded with PTX and NLG919 would efficiently penetrate into PDA tumor tissues, and high concentration of tumor intracellular GSH promotes the release of GEM, PTX and NLG919 from PGEM carrier. The biodistribution and tumor penetration of NPs were studied in PANC02 pancreatic tumor model. The antitumor activity of the combination therapy and the underlying mechanism were also investigated.

2. Materials and methods

2.1. Materials

PEOG-co-PVD and PGEM polymers were synthesized as previously reported [29]. Paclitaxel was purchased from AK Scientific

Inc. (CA, U. S. A.). Doxorubicin hydrochloride salt (DOX·HCl) were purchased from LC Laboratories (MA, USA). Pacific Blue (PB)-conjugated anti-mouse CD8 antibody (#558106) and PE-CF594-conjugated FoxP3 antibody (#9129564) were purchased from BD Company. BV785-conjugated CD4 was purchased from SIRTIGEN (#100453). PerCP-conjugated CD45 was purchased from BIOLEGEN (#103130). Penicillin-streptomycin solution and fetal bovine serum (FBS) were purchased from Invitrogen (NY, U. S. A.). All other agents were purchased from Sigma-Aldrich (MO, U. S. A.).

All animal-related experiments were performed in full compliance with institutional guidelines and approved by the Animal Use and Care Administrative Advisory Committee at the University of Pittsburgh.

2.2. Preparation and characterization of drug-loaded micelles

Drug-loaded micelles were prepared by film hydration method. PGEM polymer and drugs (e.g. PTX, curcumin, NLG919, DOX) were dissolved in methylene chloride/methanol at different weight ratios. The organic solvents were removed by nitrogen low and subsequent vacuum drying to form a thin film. Then PBS solution was added to hydrate the film to yield drug-loaded micelles. Micelles co-loaded with PTX and NLG919 were prepared in a similar way.

2.3. Formulation characterization

The average particle size, size distribution and morphology of micelles were measured by dynamic light scattering (DLS, Malvern Zeta Sizer) and transmission electron microscopy (TEM, JEOL JEM-1011). Drug loading capacity (DLC) and drug loading efficiency (DLE) were determined by HPLC (Waters).

2.4. In vitro PTX and NLG919 release

The release of PTX or NLG919 from PGEM micelles was examined at 37 °C via a dialysis method. PTX/NLG919 co-loaded PGEM micelles was transferred into a dialysis bag with MWCO of 3500 Da, which was then incubated in 50 mL PBS with 0.5% (w/v) tween 80 under gentle shaking. At specific time intervals, the PTX and NLG919 concentrations in the dialysis bag were determined by HPLC.

2.5. Cellular uptake

Pancreatic carcinoma cells PANC02 were seeded into a 6-well plate with 1 mL of Dulbecco's Modified Eagle medium (DMEM) containing 10% FBS. After 24 h, free Rhodamine and Rhodamine-loaded PGEM micelles were added into each well with a rhodamine concentration of 750 ng/mL. After incubation for 5 h, Hoechst 33,258 was added to each well at a final concentration of 5 µg/mL, and cell was further incubated at 37 °C for 15 min. Then the cells were washed with saline for three times before imaging under BZ-X710 fluorescence microscope.

2.6. MTT assay

Two murine pancreatic carcinoma cell lines PANC02 and H7 cells were seeded into a 96-well plate with 100 µL of DMEM containing 10% FBS at a density of 2000 cells/well. After incubation for 24 h, PTX-, NLG919- or PTX+NLG919-loaded micelles with various concentrations were added into the wells and incubated for another 96 h. The cell viabilities were measured by MTT assay as reported [30].

2.7. In vitro IDO inhibition

An IDO assay was used to evaluate the IDO inhibitory activity of drug-loaded micelles [14]. Briefly, PANC02 cells were seeded in a 96-well plate (5×10^3 cells/well). After culturing overnight, recombinant human IFN- γ was added to each well with concentration of 50 ng/mL. Then cells were treated with various concentrations of micellar formulations or free NLG919 for 48 h. The supernatant (150 µL) was transferred to a new 96-well plate, followed by the addition of 75 µL of 30% trichloroacetic acid. After incubation at 50 °C for 30 min, N-formylkynurenine was hydrolyzed to kynurenine. The supernatants were transferred into a new 96-well plate and treated with an equal volume of Ehrlich reagent (2% p-dimethylamino-benzaldehyde in glacial acetic acid, w/v) for 10 min for the colorimetric assay at 490 nm.

2.8. Near infrared fluorescence (NIR) imaging

To establish a syngeneic PANC02 pancreatic tumor model, 2×10^5 PANC02 cells were subcutaneously injected into the flank of C57BL/6 mice. When the tumor volume reached 200 mm³, the tumor bearing mice were intravenously injected with DiR-loaded PEOG-co-PVD and PGEM NPs at a DiR concentration of 0.5 mg/mL. At indicated time points (6 h, 15 h and 24 h), the mice were sacrificed, and the major tissues were excised, and imaged by IVIS 200 system.

2.9. In vivo PTX and NLG919 distribution

For PTX distribution study, the mice were sacrificed at 24 h after administration. The tissues were collected and homogenized with 3 parts PBS to 1 part tissue (v/g). An aliquot of 10 µL of [¹³C₆]-paclitaxel (500 ng/mL; 50 ng/mL final concentration) of internal standard solution was added to a microcentrifuge tube that contained tissue homogenate, calibrator or QC. Further sample analysis was done as previously published [31].

For NLG919 analysis, an aliquot of 10 µL of internal standard solution (50 ng/mL [D₁₀]-NLG919, Toronto Research Chemicals, ON, Canada) was added to a microcentrifuge tube that contained tissue homogenate, calibrator or QC. Next, 200 µL of diluent solution (37% acetonitrile: 63% of 10% trifluoroacetic acid in water) was added, followed by vortexing for 1 min. After centrifugation at 17,200 × g for 10 min, 3 µL of the resulting supernatant was injected into the LC-MS/MS system. The LC system consisted of an Agilent (Palo Alto, CA, USA) 1200 SL autosampler and binary pump, an Agilent SBC-18 (1.8 µm, 50 × 2.1 mm) column, and a gradient mobile phase. Mobile phase solvent A was acetonitrile with 0.1% formic acid, and mobile phase solvent B was water with 0.1% formic acid. The mobile phase composition was 30% solvent A from time 0–1.5 min, pumped at 0.4 mL/min. Solvent A was then increase linearly from 30% to 90% from 1.5 min until 4 min, where it was held till 5 min. At 5.1 min, solvent A was decreased to 30% and flow was increased to 0.5 mL/min and these conditions were held until 7 min for re-equilibration.

2.10. In vivo tumor penetration

Both PGEM and PEOG-co-PVD carriers were loaded with fluorophore rhodamine and intravenously injected into mice, respectively. Tumors were excised at 15 h after injection, and frozen sectioned at 7-µm thickness. The sections were incubated with FITC-conjugated mAb specific for blood vessel marker (CD31) overnight at 4 °C. After washing with Nano water, the section was further stained with DAPI to label the cell nucleus for fluorescence imaging. The quantitative rhodamine intensities were calculated by analyzing three different images using Image J software.

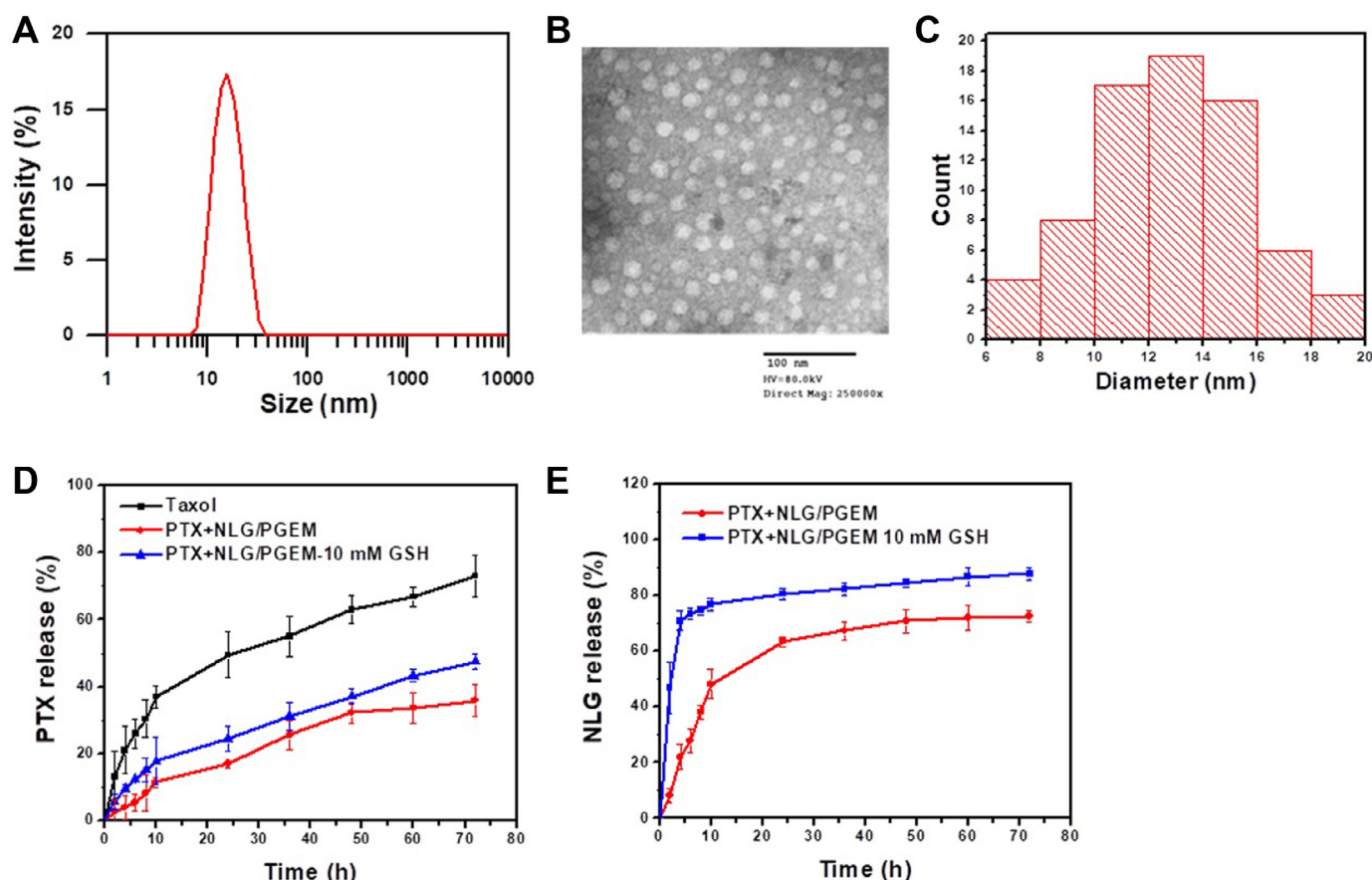


Fig. 2. The DLS size distribution (A), TEM images (B) and corresponding size histograms (C) of PTX/NLG919-co-loaded PGEM micelles. Cumulative PTX (D) and NLG919 (E) release profiles in response to 10 mM GSH. PBS containing 0.5% (w/v) Tween 80 was used as the release medium. Values reported are the means \pm SD.

2.11. In vivo therapeutic study and quantification of tumor-infiltrating lymphocytes in PANC02 model

PANC02 tumor (50 mm³)-bearing mice were randomly divided into six groups ($n = 5$) and were i.v. injected with PBS, PGEM micelles, PTX/PGEM micelles, NLG919/PGEM micelles, PTX+NLG919/PGEM micelles, and combination of Taxol, NLG919 and free GEM, respectively. The dosage of GEM, PTX and NLG919 were kept at 20 mg/kg, 10 mg/kg and 20 mg/kg. The injection was made every five days for a total of 6 times, and the tumor volume and mice body weights were measured. The tumor volume (V) were calculated by the formula: $V = (\text{length of tumor}) \times (\text{width of tumor})^2 / 2$. At 24 h following the last treatment, the mice were sacrificed and the serum levels of ALT, AST, creatinine, and BUN were measured. Meanwhile, tumor tissues and spleen were excised to acquire single cell suspensions, which were further filtered. The red blood cells were lysed and then the cells were stained with various antibodies for flow cytometry analysis with FlowJo software (Tree Star Inc.) [19].

In a separate study, the survival of the PANC02 tumor-bearing mice ($n = 8$) receiving various treatments was examined. The end point of survival was defined when the mice were deceased or when the tumor volume reached ~ 2000 mm³.

2.12. Therapeutic studies in 4T1 and CT26 models

A syngeneic 4T1 breast cancer model was established by inoculating 2×10^5 4T1 cells into right mammary fat pad of female BALB/c mice. When the tumor volume reached ~ 50 mm³, the mice were treated with various formulations as previously described for

PANC02 model. CT26 colon cancer model was established by subcutaneously inoculating 1×10^6 CT26 cells into right flank of the BALB/c-J mice. When the tumor volume reached ~ 100 mm³, the mice were i.v. administrated with various formulations.

2.13. Statistical analysis

Two-tailed Student's T test or one-way analysis of variance (ANOVA) was used to compare two groups or multiple groups, and $p < 0.05$ is considered statistically significant.

3. Results and discussion

3.1. Physicochemical characterization of PGEM micelles co-loaded with PTX and NLG919

PDA is known to have a highly immunosuppressive TME and is enriched with dense fibrotic stroma, which not only promotes the aggressiveness of PDA but also imposes difficulty in drug delivery. Therefore, there is an urgent need for rational design of immunochemo combination therapy as well as the development of a suitable formulation for selective delivery to tumors [32]. Compared to free drug combinations, engineering both chemotherapeutic and immunomodulating agents into a single nanocarrier has the advantages of improving the pharmacokinetics and biodistribution profiles, decreasing side effects and allowing the simultaneous delivery of multiple drugs to tumor site at their optimal dosages [33,34]. However, it is still a big challenge to design a carrier that is sufficiently small for penetrating the

Table 1

Characterization of PGEM micelles loaded with various drugs, including PTX, curcumin, NLG919, doxorubicin, and PTX/NLG919. (The NLG919 was shortened to NLG in the following table and figures).

Micelles	Mass ratio (mg: mg)	Size (nm) ^a	PDI ^b	DLC (%) ^c	DLE (%) ^d
PGEM	–	13.14	0.169	–	–
PGEM: PTX	2.5:1	23.07	0.265	24.2	84.6
PGEM: NLG	2.5:1	18.53	0.305	24.3	85.1
PGEM: DOX	2.5:1	22.09	0.337	25.1	88.0
PGEM: Cur	10:1	15.50	0.195	8.7	96.1
PGEM: PTX:	20:1:2	15.40	0.182	4.0 (PTX)	83.9 (PTX)
NLG				7.9 (NLG)	86.4 (NLG)

^a Measured by Zetasizer Nano ZS.

^b PDI is polydispersity index.

^c DLC is the drug loading capacity.

^d DLE is the drug loading efficiency.

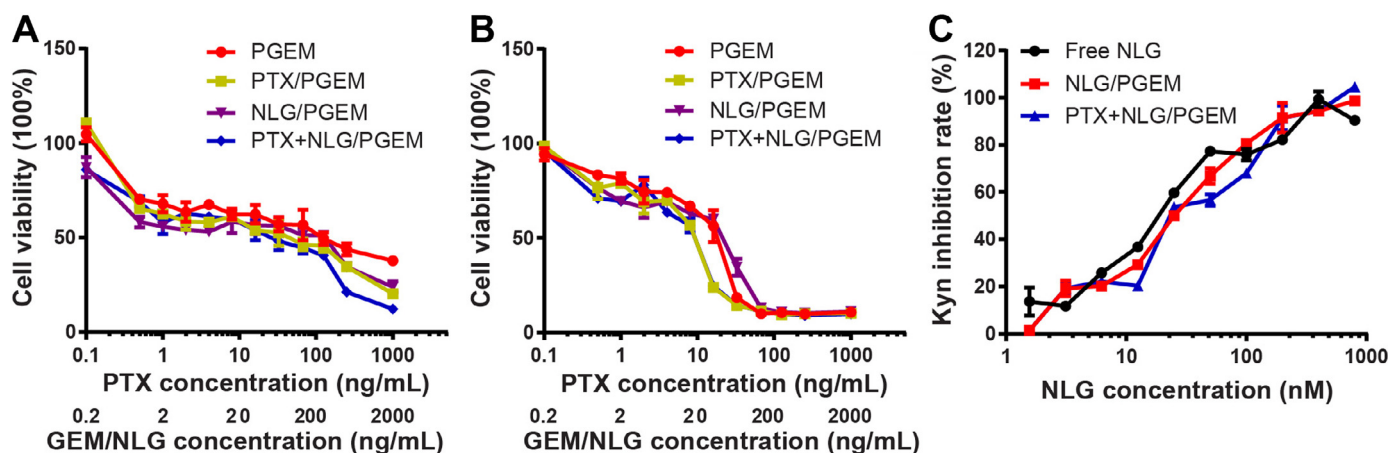


Fig. 3. *In vitro* biological activity of various formulations. MTT cytotoxicity assay of various formulations in (A) PANC02 cell line and (B) H7 cell line. Cells were treated with different micelles for 96 h. (c) Inhibitory effect of IDO activity. PANC02 cells were treated with IFN- γ together with free NLG919, NLG919/PGEM and PTX+NLG919/PGEM. Kynurenine in supernatants was measured 2 d later. All data are reported as means \pm SD.

poorly vascularized and stroma-rich PDA tumor yet effective in co-loading and codelivery of the two different therapeutic agents.

Recently, we developed a GEM-conjugated polymer PGEM, and discovered that GEM conjugation to the PEG-co-PVD polymer backbone led to a drastic decrease in the size of NPs from 160 nm to 13 nm. These ultrasmall NPs were highly effective in tumor accumulation and penetration in a colon cancer patient derived xenograft (PDX) model [29]. In this work, we evaluated if the ultra-small PGEM carrier could efficiently co-load and deliver chemotherapeutic PTX and immunostimulatory agent NLG919 into PDA tumor for effective immunochemotherapy.

As shown in Table 1, a wide variety of anti-cancer agents including PTX, curcumin, NLG919, and doxorubicin could be loaded into PGEM carrier to form ultra-small NPs. The sizes range from 14 to 23 nm with a drug loading capacity of 8%–24%. Moreover, PGEM carrier could co-encapsulate PTX and NLG919 to form small NPs with a particle size of 15.4 nm (Fig. 2A). Uniform spherical NPs were observed for PTX/NLG919 co-loaded micelles by TEM (Fig. 2B). The size histograms obtained from TEM images showed particle size distribution from 6 nm to 20 nm (Fig. 2C), which was consistent with DLS result. It has been reported that NPs with a diameter range of 4–200 nm have long circulation time and can efficiently accumulate in the tumors due to the enhanced permeability and retention (EPR) effect. NPs less than 4 nm are rapidly excreted from the kidney, while NPs larger than 200 nm tend to be taken up by the reticuloendothelial system (RES) [35]. In addition, compared to larger NPs, smaller NPs with a diameter less than 30 nm showed more efficient penetration into tumors, particularly for PDA [24,36]. The optimal size of our PTX+NLG919

co-loaded micelles shall contribute significantly to the efficient tumor accumulation and penetration as detailed later.

The stability of PTX+NLG919/PGEM micelles was evaluated by measuring the size changes under 1:10 and 1:100 dilutions. As shown in Supplementary Fig. S1, there was no obvious changes in the particle sizes under dilution conditions, suggesting good stability after intravenous injections.

The PTX and NLG919 release profiles of PTX+NLG919/PGEM micelles were evaluated with a dialysis method. As shown in Fig. 2D, Taxol showed faster release of PTX and almost 75% of PTX was released within 72 h. In comparison, PTX+NLG919/PGEM micelles showed a more favorable release kinetics of PTX, and only 35% of PTX was slowly released within 72 h. In the presence of 10 mM GSH, PTX release from PTX+NLG919/PGEM micelles was accelerated and 47% of PTX was released at 72 h. Facilitated release was similarly observed for NLG919 in response to 10 mM GSH (Fig. 2E). These results indicated that the highly redox environment in the tumor cells could promote the release of PTX and NLG919 from the carrier due to the cleavage of disulfide linkage by intracellular GSH [30].

3.2. Biological activity of PTX and NLG919 formulated in PGEM carrier

PTX and NLG919 were formulated in the PGEM carrier because PTX and GEM have been reported to have synergistic chemotherapy effect, and the IDO inhibitor NLG919 has been reported to inhibit tumor growth through reversing tumor immunosuppressive microenvironment [4,19]. First, we evaluated the cellular uptake

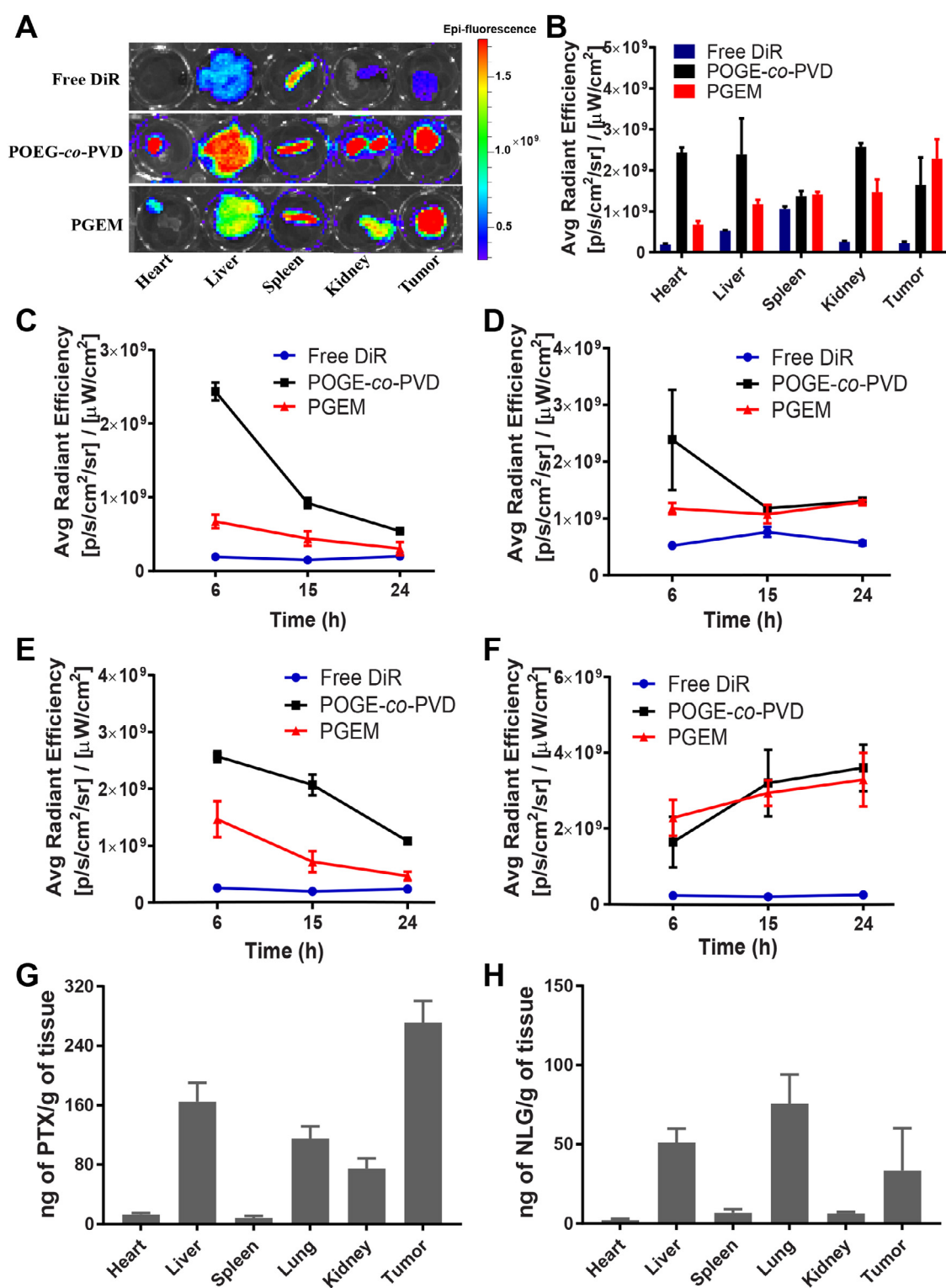


Fig. 4. Biodistribution of PGEM carrier with POEG-co-PVD carrier as a control. (A) Ex vivo NIR images of major organs and tumors of each mouse treated with DiR-labeled POEG-co-PVD (160 nm NPs) and PGEM (15 nm NPs) respectively at 6 h. (B) Quantitative analysis of the ex vivo fluorescence intensities of different organs (mean \pm S.E.M., $n = 3$). (C) The accumulation of different formulations at heart with time. (D) The accumulation of different formulations at liver with time. (E) The accumulation of different formulations at kidney with time. (F) The accumulation of different formulations at tumor with time. Tissue distribution of PTX (G) and NLG919 (H) in PANC02 tumor-bearing mice at 24 h following i.v. injection of PTX+NLG919 co-loaded PGEM micelles.

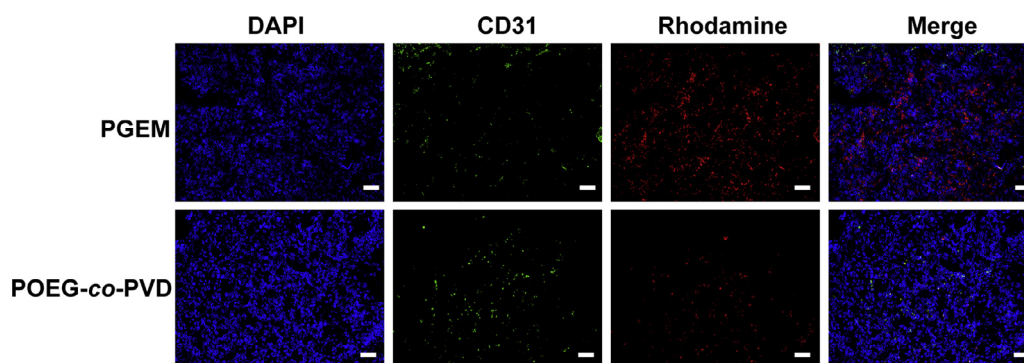


Fig. 5. Tumor penetration study. Co-localization of blood vessel (CD-31, green) and carriers (PGEM and POEG-co-PVD) labeled in red. Scale bar: 50 nm. (For interpretation of the references to color in this figure legend, the reader is referred to the web version of this article.)

of PGEM carrier with rhodamine as a fluorescence probe (Supplementary Fig. S2). Compared with free rhodamine, PGEM carrier showed similar cellular uptake at 5 h after treatment. The cytotoxicity of PGEM micelles loaded with PTX, NLG919 or PTX+NLG919 was evaluated in PANC02 cells (Fig. 3A) and H7 cells (Fig. 3B), respectively. In PANC02 cells, compared to PGEM, PTX/PGEM and NLG919/PGEM showed better cytotoxicity. Co-loading of PTX and NLG919 into PGEM further improved the cytotoxicity with a lower IC₅₀ of 14.69 ng/mL (Table S1) although the magnitude of difference was relatively small. In H7 cells, NLG919-loaded micelles showed similar cytotoxicity as compared to PGEM carrier, and both of them exhibited similar IC₅₀ (Table S1). PTX-loaded micelles and PTX/NLG919 co-loaded micelles showed improvement in cytotoxicity with lower IC₅₀ compared to PGEM and NLG919-loaded micelles, suggesting that incorporation of immunomodulatory agent NLG919 didn't change the cell killing effect of PGEM in H7 cells, while incorporation of chemotherapeutic PTX in the formulation enhanced the cell killing effect. The relatively limited synergy between PGEM and PTX is likely due to the incomplete release of GEM in the cultured cells during the short period of time.

The IDO inhibitory activity of the formulations NLG919/PGEM and PTX+NLG919/PGEM was investigated in PANC02 cells by detecting the decreased levels of kynurenine (Kyn) through a colorimetric assay [19]. Fig. 3C shows the Kyn inhibition rates in PANC02 cells after the treatment with free NLG919, NLG919/PGEM and PTX+NLG919/PGEM at various NLG919 concentrations. They all inhibited the IDO activity in an NLG919 concentration dependent manner. NLG919/PGEM and PTX+NLG919/PGEM formulations showed similar levels of IDO inhibition compared to free NLG919. This result suggested that NLG919 formulated in the PGEM carrier well maintained its biological effect in inhibiting the IDO activity, and co-delivery of PTX with NLG919 didn't affect the IDO inhibitory effect of NLG919.

3.3. Biodistribution and tumor penetration

In vivo biodistribution of PGEM carrier was evaluated in PANC02 tumor model by near-infrared fluorescent optical imaging using IVIS system with the larger-sized POEG-co-PVD carrier without GEM motifs (~160 nm) as a control. The mice were i.v. administered with DiR/PGEM and DiR/POEG-co-PVD, respectively. Major organs including the heart, liver, spleen, kidney and tumor were excised at 6, 15 and 24 h for ex vivo imaging. At 6 h post injection (Fig. 4A), very weak fluorescence signals were observed in these organs except kidney after treatment with free DiR. DiR-loaded POEG-co-PVD micelles group showed strong fluorescence intensities in all of the tested organs, while DiR-loaded PGEM micelles only showed strong fluorescence intensities in the spleen

and tumor. Fig. 4B showed quantitative analysis of fluorescence intensities in different tissues. DiR-loaded PGEM micelles showed higher accumulation in the tumor tissue than in the other organs. Similar results were obtained at 15 h (Supplementary Fig. S3) and 24 h (Supplementary Fig. S4) post injection, respectively. Fig. 4C–F showed the accumulation of various formulations in different organs at various time points. For both DiR/POEG-co-PVD- and DiR/PGEM-treated groups, fluorescence intensities decreased in heart and kidney, and increased in the tumors over time. Compared to free DiR, both micelles showed higher accumulation in the tumors, suggesting the advantages of micellar formulation in improving tumor uptake due to the EPR effect. Although PGEM micelles didn't show significant enhancement in tumor uptake compared to POEG-co-PVD micelles, it did show lower uptake by heart and kidney at all time points (6, 15 and 24 h). In addition, significant less accumulation in liver was found for PGEM micelles at early time point (6 h) compared to POEG-co-PVD micelles.

The tissue distribution of PTX and NLG919 formulated in PGEM NPs was evaluated in PANC02 tumor-bearing mice to confirm that PGEM was similarly effective in targeted delivery of therapeutic agents to tumors as it did with fluorescence probes. Much more PTX was found in tumors compared to those accumulated in a number of normal organs examined including heart, liver, spleen, lung and kidney (Fig. 4G). More NLG919 was delivered into tumor, liver and lung compared to other organs (Fig. 4H). These data suggested that PGEM carrier could efficiently co-deliver both PTX and NLG919 into tumors, indicating the advantage of the small sized PGEM in the tumor accumulation. The less tumor targeting efficiency of NLG919 compared to PTX might be due to the faster release of NLG919 from the PGEM NPs (Fig. 2E). However, a fast degradation of NLG919 in tumor tissues can't be ruled out, which warrants more studies in the future.

It has been reported that NPs with smaller size showed deeper penetration in PDA tumor [24]. Thus, the tumor penetration capability of the smaller PGEM carrier was compared to that of larger POEG-co-PVD NPs in PANC02 tumor model. Both PGEM and POEG-co-PVD carriers were labeled with fluorophore rhodamine and intravenously injected into mice. Tumor sections were collected at 15 h and co-stained with FITC-conjugated mAb specific for blood vessel marker CD31. As shown in Fig. 5, the red rhodamine signals from POEG-co-PVD carrier were overlapped with green signals, indicating the POEG-co-PVD micelles stayed at or near the tumor blood vessels. For PGEM carrier, most red signals spread from the blood vessels, suggesting a better penetration capability. Fig. S5 shows the co-localization images of other tumor areas and quantitative rhodamine fluorescence intensities, further confirming the better penetration capability of PGEM.

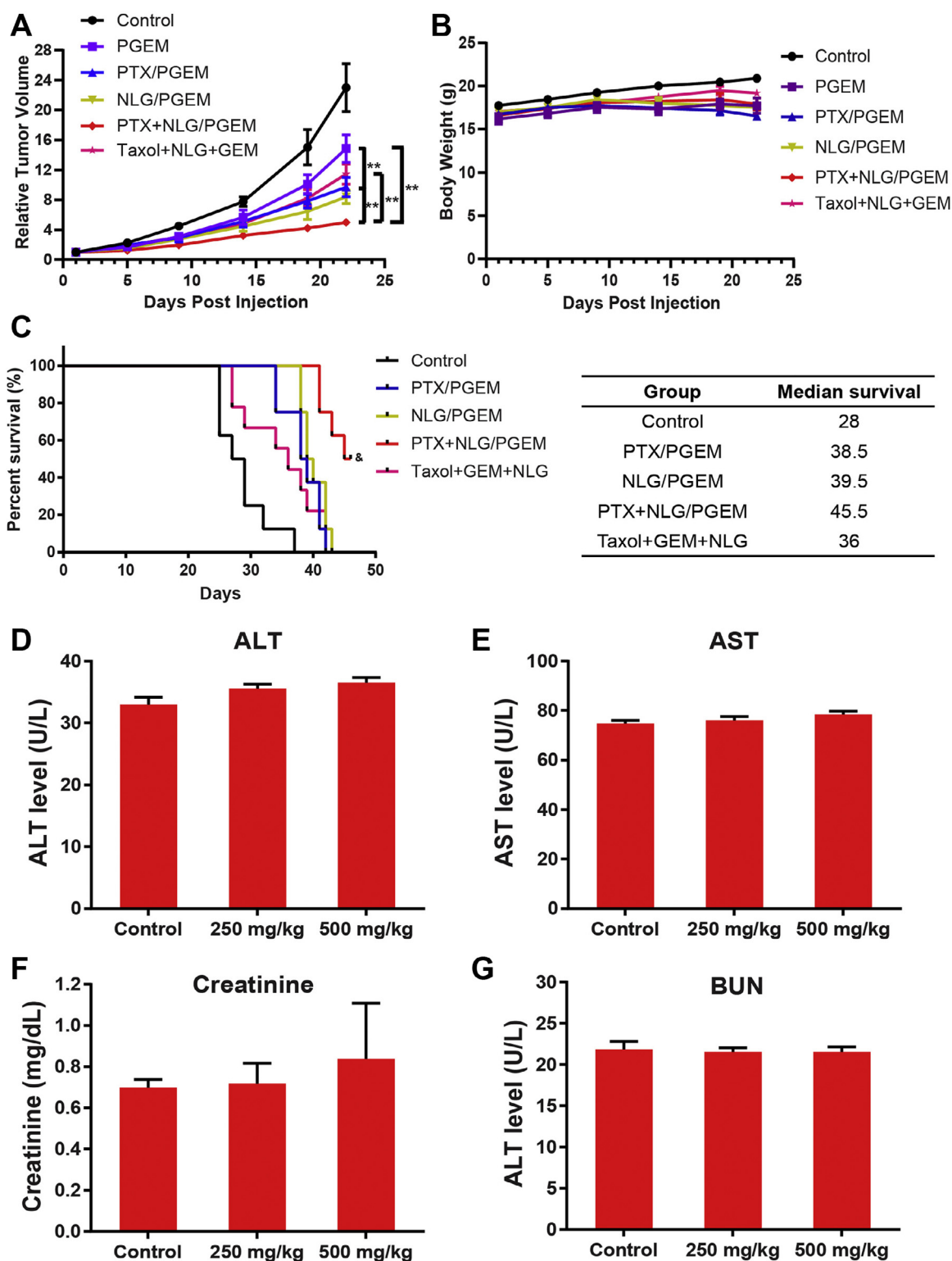


Fig. 6. *In vivo* therapeutic effect and safety profiles in PANC02 model. Relative tumor volume changes (A) and survival rate (B) of the mice treated with various formulations. Serum levels of alanine aminotransferase (ALT, D) and aspartate aminotransferase (AST, E), creatinine (F) and blood urea nitrogen (BUN, G) in mice from control and PTX+NLG919/PGEM NPs (at PGEM dosage of 250 mg/kg and 500 mg/kg; the dosage of GEM was 20 mg/kg and 40 mg/kg, respectively)-treated groups. ***p* < 0.01.

3.4. *In vivo* therapeutic study in PANC02 model

To study the combination effect of immunotherapy with chemotherapy in PDA, an immunocompetent murine model of pancreatic cancer (PANC02) was used. PANC02 is reported to be highly resistant to chemotherapeutic drugs and, therefore,

can be used to closely mimic human PDA [37,38]. The PANC02 tumor-bearing mice were i.v. administered with saline, PGEM carrier, PTX/PGEM, NLG919/PGEM, PTX+NLG919/PGEM micelles and Taxol+GEM+NLG919 combination. As shown in Fig. 6A, PGEM carrier itself could inhibit tumor growth, and introduction of PTX or NLG919 into PGEM carrier further improved the anti-tumor

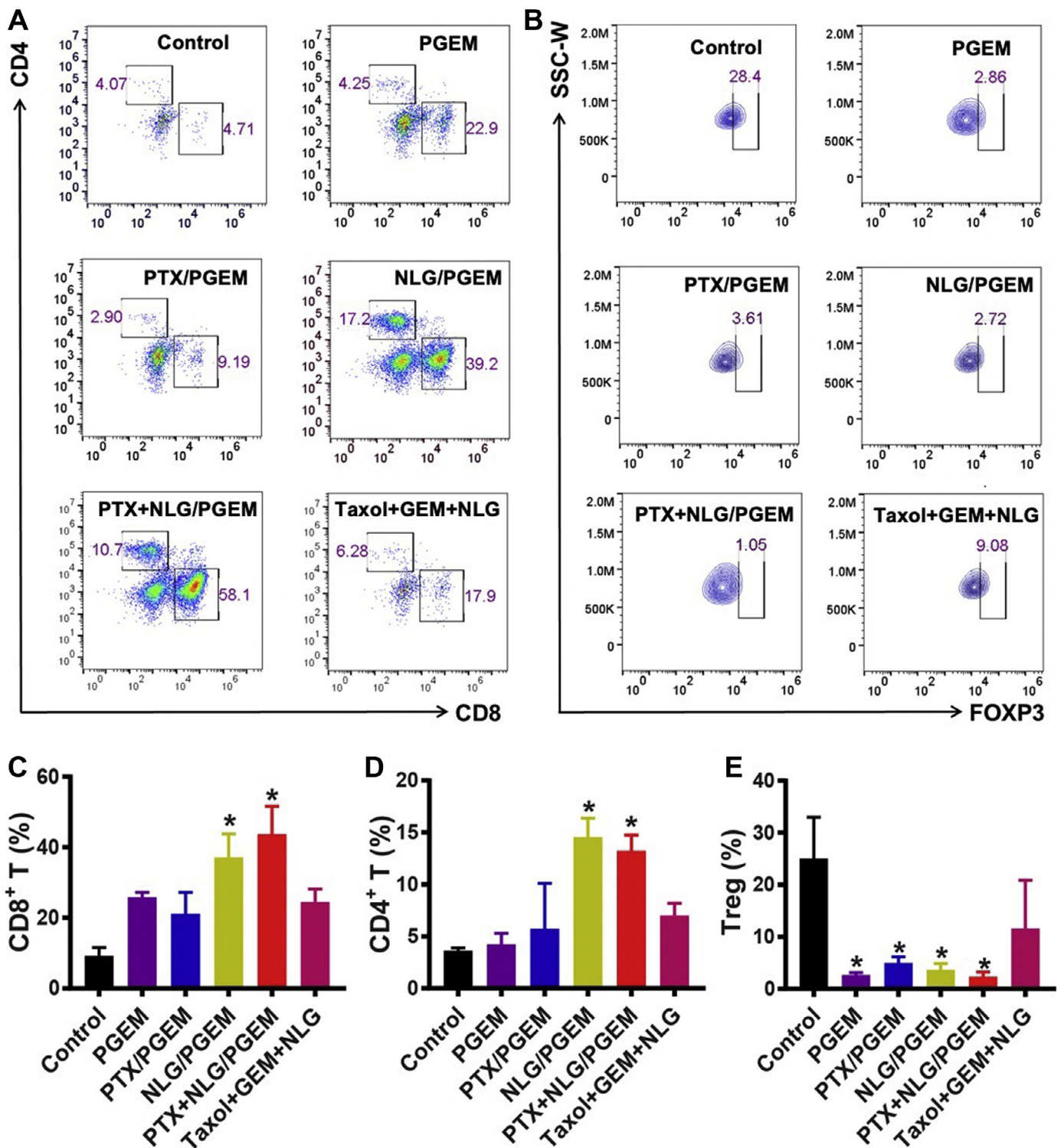


Fig. 7. The mechanism study by flow cytometry. Representative flow cytometry gatings of tumor infiltrating immune cells after various treatments, including (A) CD4⁺ T cells and CD8⁺ T cells, as well as (B) regulatory T (Treg) cells. The percentage of tumor infiltrating (C) CD8⁺ T cells and (D) CD4⁺ T cells in the tumor tissues and (E) the percentage of Treg cells in the total CD4⁺ T cells was correspondingly quantified. The results are reported as mean \pm S.E.M. * $p < 0.05$ (vs. Control).

activity. Among all the formulations, PTX+NLG919/PGEM micelles showed the highest anti-tumor activity (** $p < 0.01$ vs. control, PGEM, PTX/PGEM and Taxol+GEM+NLG919), suggesting incorporation of both chemotherapeutic PTX and immunomodulatory agent NLG919 into PGEM micelles is the best combination group. No significant changes in body weights were noticed in all treatment groups (Fig. 6B).

The survival of the mice receiving various treatments was further investigated. Compared to control group, mice treated with PTX/PGEM and NLG919/PGEM had an increased survival rate with a median survival time of 38.5 and 39.5 days, respectively (Fig. 6C). Moreover, treatment of PTX+NLG919/PGEM micelles significantly increased survival time (45.5 days) compared to PTX/PGEM, NLG919/PGEM and Taxol+GEM+NLG919 combination. Due to the

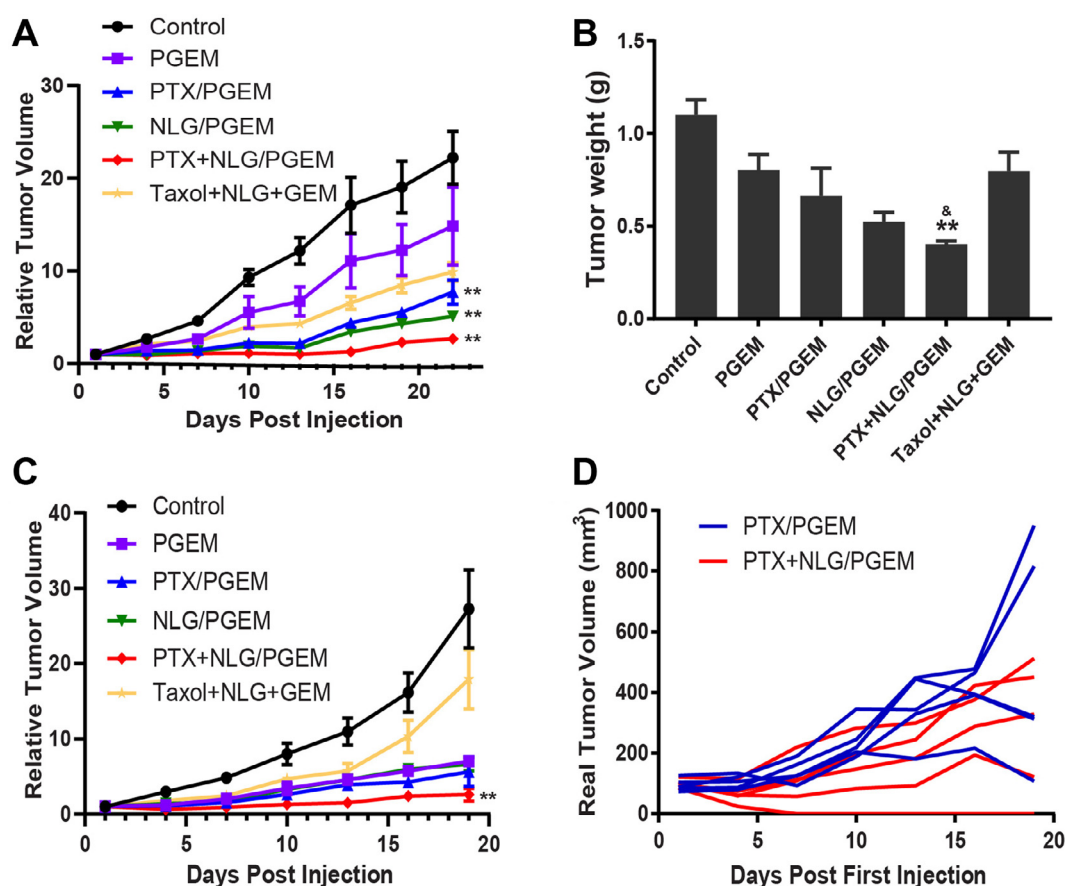


Fig. 8. *In vivo* therapeutic effect in other tumor models, including 4T1 and CT26 models. (A) Relative tumor volume changes of the 4T1 tumor-bearing mice treated with various formulations. (B) 4T1 tumor weights of the mice receiving different treatments. (C) Relative tumor volume changes of the CT26 tumor-bearing mice treated with various formulations. (D) The individual CT26 tumor growth after treatment with PTX/PGEM and PTX+NLG919/PGEM. The results are reported as mean \pm S.E.M. * $p < 0.05$, ** $p < 0.01$ (vs. Control); $^{\&}p < 0.05$ (vs. PGEM).

severely ulcerated tumors, we had to sacrifice the mice at 46 days (marked as &) before they reached the maximum allowable size. These results suggested the therapeutic benefit of combining immunotherapy with chemotherapy using PTX+NLG919/PGEM micelles.

The biochemical parameters including serum levels of alanine aminotransferase (ALT), aspartate aminotransferase (AST), creatinine and blood urea nitrogen (BUN) following the treatment of PTX+NLG919/PGEM micelles (with PGEM dosage of 250 mg/kg or 500 mg/kg) were evaluated as indicators of hepatic and renal function. As shown in Fig. 6D–G, no significant changes were noticed for any of these parameters, suggesting that our formulations were well tolerated at the dosages used.

3.5. The anti-tumor immune response of various formulations

The populations of infiltrated T cells in the tumors following various treatments were investigated by flow cytometry (Figs. 7 and S6). PGEM treatment could increase the relative populations of CD8⁺ T cells in the tumors, and decrease the relative populations of Treg cells in the total CD4⁺ T cells. There was no significant changes in CD8⁺ T cells and Treg cells after treatment with PTX/PGEM micelles compared to PGEM treatment, indicating incorporation of PTX into PGEM carrier didn't affect the immune response induced by PGEM, and the improved therapeutic effect of PTX/PGEM micelles was mainly attributed to the synergistic tumor killing effect of PTX with GEM [39]. Compared to PGEM carrier, NLG919/PGEM and PTX+NLG919/PGEM micelles shows better

effect in stimulating the CD8⁺ and CD4⁺ T cell response, as well as inhibiting the Treg cell response, which generated a more active tumor immune microenvironment. Since incorporation of NLG919 didn't improve the cytotoxicity of PGEM (Fig. 3B), the enhanced therapeutic effect of NLG919/PGEM with respect to PGEM was likely attributed to the enhanced immune system. In addition, PTX+NLG919/PGEM was more effective in boosting anti-tumor immune response compared with Taxol+GEM+NLG919 combination, which might be explained by the more effective delivery of PTX/GEM/NLG919 into the tumors through the ultra-small sized carrier.

There are no significant differences in the immune profiles between NLG919/PGEM and PTX+NLG919/PGEM. Although incorporation of PTX didn't improve the anti-tumor immunity of NLG919/PGEM, it did improve the overall antitumor activity through the synergistic tumor killing effect of PTX with GEM. The fact that PTX+NLG919/PGEM has the highest level of anti-tumor activity suggests the necessity of the combination of PTX-mediated chemotherapy and NLG919-mediated immunotherapy. In fact, a new study of combining indoximod (another IDO inhibitor) with chemotherapeutics including nab-PTX and GEM for advanced PDA has moved into phase Ib trial (NCT02077881). In this work, we have also demonstrated that co-delivery of the potent IDO1 inhibitor (NLG919) and chemotherapeutics (PTX and GEM) via the tumor permeable nanocarrier is highly efficacious for the treatment of pancreatic cancer in PANC02 model, which is more effective than Taxol+GEM+NLG919 combination. To extend the application of PTX+NLG919/PGEM regimen, future studies

will investigate its therapeutic efficacy in other mouse models of pancreatic cancer such as a genetically engineered mouse model.

3.6. Therapy effect against other tumor models

The therapeutic effect of PTX+NLG919/PGEM micelles was also investigated in 4T1.2 (breast) and CT26 (colon) tumor models. PGEM carrier alone showed anti-tumor effect in 4T1.2 model (Fig. 8A). Incorporation of PTX or NLG919 into PGEM carrier further enhanced the anti-tumor effect. Among all the groups, the treatment with PTX/NLG919-co-loaded PGEM micelles led to the best anti-tumor effect (Fig. 8B). Compared to 4T1.2 model, PGEM carrier alone was more effective in inhibiting the tumor growth in CT26 model (Fig. 8C). In CT26 model, PGEM was much more effective than the combination group of Taxol+GEM+NLG919. Mice treated with PTX+NLG919/PGEM showed the lowest tumor growth, and the tumor in one mouse had completely regressed at day 7 after the first treatment (Figs. 8D and S7). Besides, all the formulations were safe in these models, and no significant changes were observed in the body weights of the treated mice. These data suggested that PTX+NLG919/PGEM micelles may find a broad application in treating various types of cancers including PDA.

4. Conclusion

This work has provided a new immunochemotherapy regimen for enhanced PDA treatment by incorporation of PTX and NLG919 into PGEM carrier to synergistically kill tumor cells and reverse IDO-mediated immunosuppression. We demonstrated that PGEM carrier could co-load PTX and NLG919 to form micelles with small particle size and was effective in delivering both drugs to the tumor tissues. *In vivo* studies showed that incorporation of NLG919 into the carrier induced a more immunoactive tumor microenvironment with increased CD8⁺ T cells and decreased Treg cells, and thereby enhanced the therapeutic effect. Co-delivery of PTX and NLG919 through the nanocarrier further enhanced the therapeutic effect in PDA tumors by significantly inhibiting the tumor growth and prolonging the survival rate, which was more effective than Taxol+GEM+NLG919 combination. In addition to PDA, PTX+NLG919/PGEM micelles were also effective in inhibiting tumor growth in other tumor models, suggesting its wide application.

Declaration of Competing Interest

The authors declare that they have no known competing financial interests or personal relationships that could have appeared to influence the work reported in this paper.

Acknowledgments

This work was supported by National Institute of Health grants R01CA174305, R01CA219399, R01CA223788 (S Li), R50 CA211241 (R Parise) and a grant from Shear Family Foundation. The biodistribution study was performed using the UPMC Hillman Cancer Center Cancer Pharmacokinetics and Pharmacodynamics Facility (CPPF) and was supported in part by award P30-CA47904.

Supplementary materials

Supplementary material associated with this article can be found, in the online version, at doi:[10.1016/j.actbio.2020.01.039](https://doi.org/10.1016/j.actbio.2020.01.039).

References

- [1] L. Rahib, B.D. Smith, R. Aizenberg, A.B. Rosenzweig, J.M. Fleshman, L.M. Matrisian, Projecting cancer incidence and deaths to 2030: the unexpected burden of thyroid, liver, and pancreas cancers in the united states, *Cancer Res.* 74 (11) (2014) 2913–2921.
- [2] H. Burris 3rd, M.J. Moore, J. Andersen, M.R. Green, M.L. Rothenberg, M.R. Modiano, M.C. Cripps, R.K. Portenoy, A.M. Storniolo, P. Tarassoff, Improvements in survival and clinical benefit with gemcitabine as first-line therapy for patients with advanced pancreas cancer: a randomized trial, *J. Clin. Oncol.* 15 (6) (1997) 2403–2413.
- [3] L.A. Shipley, T.J. Brown, J.D. Cornpropst, M. Hamilton, W.D. Daniels, H.W. Culp, Metabolism and disposition of gemcitabine, and oncolytic deoxycytidine analog, in mice, rats, and dogs, *Drug Metab. Dispos.* 20 (6) (1992) 849–855.
- [4] K.K. Frese, A. Neesse, N. Cook, T.E. Bapiro, M.P. Lolkema, D.I. Jodrell, D.A. Tuveson, nab-Paclitaxel potentiates gemcitabine activity by reducing cytidine deaminase levels in a mouse model of pancreatic cancer, *Cancer Discov.* 2 (3) (2012) 260–269.
- [5] N. Awasthi, C. Zhang, A.M. Schwarz, S. Hinz, C. Wang, N.S. Williams, M.A. Schwarz, R.E. Schwarz, Comparative benefits of Nab-paclitaxel over gemcitabine or polysorbate-based docetaxel in experimental pancreatic cancer, *Carcinogenesis* 34 (10) (2013) 2361–2369.
- [6] L. Zitvogel, L. Apetoh, F. Ghiringhelli, G. Kroemer, Immunological aspects of cancer chemotherapy, *Nat. Rev. Immunol.* 8 (1) (2008) 59–73.
- [7] L. Apetoh, F. Ghiringhelli, A. Tesniere, M. Obeid, C. Ortiz, A. Criollo, G. Mignot, M.C. Maiuri, E. Ullrich, P. Saulnier, Toll-like receptor 4-dependent contribution of the immune system to anticancer chemotherapy and radiotherapy, *Nat. Med.* 13 (9) (2007) 1050.
- [8] M.S. Sasso, G. Lollo, M. Pitorre, S. Solito, L. Pinton, S. Valpione, G. Bastiat, S. Mandruzzato, V. Bronte, I. Marigo, Low dose gemcitabine-loaded lipid nanocapsules target monocytic myeloid-derived suppressor cells and potentiate cancer immunotherapy, *Biomaterials* 96 (2016) 47–62.
- [9] K. Thind, L.J. Padnos, R.K. Ramanathan, M.J. Borad, Immunotherapy in pancreatic cancer treatment: a new frontier, *Therap. Adv. Gastroenterol.* 10 (1) (2017) 168–194.
- [10] N. Martinez-Bosch, J. Vinaixa, P. Navarro, Immune evasion in pancreatic cancer: from mechanisms to therapy, *Cancers* 10 (1) (2018) 6.
- [11] C. Uytendhove, L. Pilote, I. Théate, V. Stroobant, D. Colau, N. Parmentier, T. Boon, B.J. Van den Eynde, Evidence for a tumoral immune resistance mechanism based on tryptophan degradation by indoleamine 2, 3-dioxygenase, *Nat. Med.* 9 (10) (2003) 1269.
- [12] J. Godin-Ethier, L.-A. Hanafi, C.A. Piccirillo, R. Lapointe, Indoleamine 2, 3-dioxygenase expression in human cancers: clinical and immunologic perspectives, *Clin. Cancer Res.* 17 (22) (2011) 6985–6991.
- [13] H.K. Koblisch, M.J. Hansbury, K.J. Bowman, G. Yang, C.L. Neilan, P.J. Haley, T.C. Burn, P. Waeltz, R.B. Sparks, E.W. Yue, Hydroxylamine inhibitors of indoleamine-2, 3-dioxygenase potentially suppress systemic tryptophan catabolism and the growth of IDO-expressing tumors, *Mol. Cancer Ther.* 9 (2) (2010) 489–498.
- [14] X. Liu, N. Shin, H.K. Koblisch, G. Yang, Q. Wang, K. Wang, L. Leffert, M.J. Hansbury, B. Thomas, M. Rupa, Selective inhibition of IDO1 effectively regulates mediators of antitumor immunity, *Blood* 115 (17) (2010) 3520–3530.
- [15] A. Witkiewicz, T.K. Williams, J. Cuzzitorto, B. Durkan, S.L. Showalter, C.J. Yeo, J.R. Brody, Expression of indoleamine 2, 3-dioxygenase in metastatic pancreatic ductal adenocarcinoma recruits regulatory T cells to avoid immune detection, *J. Am. Coll. Surg.* 206 (5) (2008) 849–854.
- [16] D.H. Munn, A.L. Mellor, Indoleamine 2, 3-dioxygenase and tumor-induced tolerance, *J. Clin. Invest.* 117 (5) (2007) 1147–1154.
- [17] D.H. Munn, A.L. Mellor, IDO in the tumor microenvironment: inflammation, counter-regulation, and tolerance, *Trends Immunol.* 37 (3) (2016) 193–207.
- [18] A. Nayak, Z. Hao, R. Sadek, N. Vahanian, W.J. Ramsey, E. Kennedy, M. Mautino, C. Link, P. Bourbo, R. Dobbins, A phase I study of NLG919 for adult patients with recurrent advanced solid tumors, *J. Immunother. Cancer* 2 (S3) (2014) P250.
- [19] Y. Chen, R. Xia, Y. Huang, W. Zhao, J. Li, X. Zhang, P. Wang, R. Venkataraman, J. Fan, W. Xie, X. Ma, B. Lu, S. Li, An immunostimulatory dual-functional nanocarrier that improves cancer immunochemotherapy, *Nat. Commun.* 7 (2016) 13443.
- [20] H. Maeda, H. Nakamura, J. Fang, The EPR effect for macromolecular drug delivery to solid tumors: improvement of tumor uptake, lowering of systemic toxicity, and distinct tumor imaging *in vivo*, *Adv. Drug Deliv. Rev.* 65 (1) (2013) 71–79.
- [21] M.K. Danquah, X.A. Zhang, R.I. Mahato, Extravasation of polymeric nanomedicines across tumor vasculature, *Adv. Drug Deliv. Rev.* 63 (8) (2011) 623–639.
- [22] F. Danhier, O. Feron, V. Préat, To exploit the tumor microenvironment: passive and active tumor targeting of nanocarriers for anti-cancer drug delivery, *J. Control. Release* 148 (2) (2010) 135–146.
- [23] V.P. Chauhan, R.K. Jain, Strategies for advancing cancer nanomedicine, *Nat. Mater.* 12 (11) (2013) 958–962.
- [24] H. Cabral, Y. Matsumoto, K. Mizuno, Q. Chen, M. Murakami, M. Kimura, Y. Terada, M. Kano, K. Miyazono, M. Uesaka, Accumulation of sub-100nm polymeric micelles in poorly permeable tumours depends on size, *Nat. Nanotechnol.* 6 (12) (2011) 815–823.

- [25] Z. Popović, W. Liu, V.P. Chauhan, J. Lee, C. Wong, A.B. Greytak, N. Insin, D.G. Nocera, D. Fukumura, R.K. Jain, A nanoparticle size series for *in vivo* fluorescence imaging, *Angew. Chem. Int. Ed.* 49 (46) (2010) 8649–8652.
- [26] V.P. Chauhan, Z. Popović, O. Chen, J. Cui, D. Fukumura, M.G. Bawendi, R.K. Jain, Fluorescent nanorods and nanospheres for real-time *in vivo* probing of nanoparticle shape-dependent tumor penetration, *Angew. Chem. Int. Ed.* 50 (48) (2011) 11417–11420.
- [27] J. Sun, Y. Chen, K. Li, Y. Huang, X. Fu, X. Zhang, W. Zhao, Y. Wei, L. Xu, P. Zhang, R. Venkataramanan, S. Li, A prodrug micellar carrier assembled from polymers with pendant farnesyl thiosalicylic acid moieties for improved delivery of paclitaxel, *Acta Biomater.* 43 (2016) 282–291.
- [28] R. Bruni, P. Possenti, C. Bordinon, M. Li, S. Ordanini, P. Messa, M.P. Rastaldi, F. Cellesi, Ultrasmall polymeric nanocarriers for drug delivery to podocytes in kidney glomerulus, *J. Control. Release* 255 (2017) 94–107.
- [29] J. Sun, Y. Chen, J. Xu, X. Song, Z. Wan, Y. Du, W. Ma, X. Li, L. Zhang, S. Li, High loading of hydrophobic and hydrophilic agents via small immunostimulatory carrier for enhanced tumor penetration and combinational therapy, *Theranostics* 10 (3) (2020) 1136–1150.
- [30] J. Sun, Y. Liu, Y. Chen, W. Zhao, Q. Zhai, S. Rathod, Y. Huang, S. Tang, Y.T. Kwon, C. Fernandez, Doxorubicin delivered by a redox-responsive dasatinib-containing polymeric prodrug carrier for combination therapy, *J. Control. Release* 258 (2017) 43–55.
- [31] S.M. Christner, R.A. Parise, P.S. Ivy, H. Tawbi, E. Chu, J.H. Beumer, Quantitation of paclitaxel, and its 6- α -OH and 3- β -OH metabolites in human plasma by LC-MS/MS, *J. Pharm. Biomed. Anal.* 172 (2019) 26–32.
- [32] P.R. Kunk, T.W. Bauer, C.L. Slingluff, O.E. Rahma, From bench to bedside a comprehensive review of pancreatic cancer immunotherapy, *J. Immunother. Cancer* 4 (1) (2016) 14.
- [33] Y. Zhao, D.Y. Alakhova, A.V. Kabanov, Can nanomedicines kill cancer stem cells? *Adv. Drug Deliv. Rev.* 65 (13–14) (2013) 1763–1783.
- [34] J. Sun, Y. Chen, Y. Huang, W. Zhao, Y. Liu, R. Venkataramanan, B. Lu, S. Li, Programmable co-delivery of the immune checkpoint inhibitor NLG919 and chemotherapeutic doxorubicin via a redox-responsive immunostimulatory polymeric prodrug carrier, *Acta Pharmacol. Sin.* 38 (6) (2017) 823–834.
- [35] G.M. Soliman, A. Sharma, D. Maysinger, A. Kakkar, Dendrimers and miktoarm polymers based multivalent nanocarriers for efficient and targeted drug delivery, *Chem. Commun.* 47 (34) (2011) 9572–9587.
- [36] J. Wang, W. Mao, L.L. Lock, J. Tang, M. Sui, W. Sun, H. Cui, D. Xu, Y. Shen, The role of micelle size in tumor accumulation, penetration, and treatment, *ACS Nano* 9 (7) (2015) 7195–7206.
- [37] L. Partecke, M. Sendler, A. Kaeding, F. Weiss, J. Mayerle, A. Dummer, T. Nguyen, N. Albers, S. Speerforck, M. Lerch, A syngeneic orthotopic murine model of pancreatic adenocarcinoma in the C57/BL6 mouse using the Panc02 and 6606PDA cell lines, *Eur. Surg. Res.* 47 (2) (2011) 98–107.
- [38] B.-F. Pan, T.S. Priebe, J.A. Nelson, Mechanisms of resistance to 6-thioguanine in a murine pancreatic tumor, *Cancer Chemother. Pharmacol.* 29 (6) (1992) 471–474.
- [39] H. Meng, M. Wang, H. Liu, X. Liu, A. Situ, B. Wu, Z. Ji, C.H. Chang, A.E. Nel, Use of a lipid-coated mesoporous silica nanoparticle platform for synergistic gemcitabine and paclitaxel delivery to human pancreatic cancer in mice, *ACS Nano* 9 (4) (2015) 3540–3557.